Molecules and Cells

Deup1 Expression Interferes with Multiciliated Differentiation

Miram Shin[1,3], Jiyeon Lee[1,3], Haeryung Lee[1,3], Vijay Kumar[2], Jaebong Kim[2], and Soochul Park[1,*]

[1]Department of Biological Sciences, Sookmyung Women's University, Seoul 04310, Korea, [2]Department of Biochemistry, Institute of Cell Differentiation and Aging, College of Medicine, Hallym University, Chuncheon 24252, Korea, [3]These authors contributed equally to this work.
*Correspondence: scpark@sookmyung.ac.kr
https://doi.org/10.14348/molcells.2023.0149
www.molcells.org

A recent study revealed that the loss of Deup1 expression does not affect either centriole amplification or multicilia formation. Therefore, the deuterosome *per se* is not a platform for amplification of centrioles. In this study, we examine whether gain-of-function of Deup1 affects the development of multiciliated ependymal cells. Our time-lapse study reveals that deuterosomes with an average diameter of 300 nm have two different fates during ependymal differentiation. In the first instance, deuterosomes are scattered and gradually disappear as cells become multiciliated. In the second instance, deuterosomes self-organize into a larger aggregate, called a deuterosome cluster (DC). Unlike scattered deuterosomes, DCs possess centriole components primarily within their large structure. A characteristic of DC-containing cells is that they tend to become primary ciliated rather than multiciliated. Our *in utero* electroporation study shows that DCs in ependymal tissue are mostly observed at early postnatal stages, but are scarce at late postnatal stages, suggesting the presence of DC antagonists within the differentiating cells. Importantly, from our bead flow assay, ectopic expression of Deup1 significantly impairs cerebrospinal fluid flow. Furthermore, we show that expression of mouse Deup1 in Xenopus embryos has an inhibitory effect on differentiation of multiciliated cells in the epidermis. Taken together, we conclude that the DC formation of Deup1 in multiciliated cells inhibits production of multiple centrioles.

Keywords: basal bodies, deup1, deuterosome, ependymal cell, lateral wall, multiciliated cell

INTRODUCTION

The ependymal cells are multiciliated cells (MCCs) that line the brain ventricles, and in these cells, the coordinated movement of the cilia is crucial for generation of a directed and strong flow of the cerebrospinal fluid (CSF) (Banizs et al., 2005; Ohata et al., 2014; Spassky and Meunier, 2017; Spassky et al., 2005). This functional property is due to the fact that ependymal precursors are able to produce large numbers of centrioles, which are then translocated to the cell's apical surface and become basal bodies (BBs) (Anderson and Brenner, 1971; Vladar and Stearns, 2007; Zhao et al., 2013). BBs serve as templates for production of multiple motile cilia and are necessary for continuous movement of the motile cilia (Fliegauf et al., 2007; Gomperts et al., 2004).

During ependymal differentiation, it is essential to understand how precursor cells with two parent centrioles generate an average of 55 centrioles per cell before nucleating multiple cilia. There have been two proposed models for this massive centriole amplification (Shahid and Singh, 2018). The first model involves parental centrioles being responsible for generating multiple daughter centrioles (Al Jord et al., 2014). The second model involves a deuterosome-dependent path-

Received September 12, 2023; revised October 1, 2023; accepted October 18, 2023; published online November 8, 2023

eISSN: 0219-1032

way responsible for generation of centrioles (Klos Dehring et al., 2013; Revinski et al., 2018; Zhao et al., 2013; 2019). These deuterosomes are electron-dense and donut-like structures found in MCCs and function as platforms for formation of centrioles, although it is not yet known whether their origin is dependent on their parental centrioles.

Deup1, a paralog of Cep63, is a key component of the aforementioned deuterosomes (Sir et al., 2011), and the knockdown of Deup1 is critical for reduction of the electron-dense deuterosomes (Zhao et al., 2013). A recent study has shown that ependymal cells lacking deuterosomes as a result of ablation of Deup1 gene are still capable of producing a large number of BBs (Mercey et al., 2019b). Moreover, cells lacking parent centrioles and deuterosomes can amplify the correct number of centrioles (Mercey et al., 2019a; 2019b). As such, there is a strong possibility that massive centriole production is not dependent on parental centrioles or deuterosomes, but may instead require another self-organizing process involving pericentriolar materials. In this regard, Deup1's role in centriole amplification in ependymal cells was reconsidered.

In this study, we used a gain-of-function approach to examine whether Deup1 plays a role in controlling centriole number in ependymal differentiation. According to our data from GFP-Deup1 experiments, deuterosomes can self-organize into large clusters, which then interfere with the proper development of BBs and hamper with the directed flow of CSF.

MATERIALS AND METHODS

DNA vectors

We obtained the GFP-Deup1 construct from the State Key Laboratory of Cell Biology (Zhao et al., 2013), made from the full sequence of Deup1 cDNA (GenBank accession No. KC211186) having been inserted into pEGFP-C2 to express GFP-tagged Deup1. The control plasmid pCAG-mGFP was a gift from Connie Cepko (Addgene plasmid #14757) (Matsuda and Cepko, 2007).

Primary ependymal cell culture and immunocytochemistry

A primary ependymal cell culture was made using brains of postnatal day 1-2 (P1-P2) mice. Dissection of the lateral walls was conducted as described previously (Delgehyr et al., 2015; Park et al., 2019). Briefly, the hippocampus, medial wall, choroid plexus, and part of the cortex were removed in Hank's solution (1XHBSS, 14170112; Gibco, USA). By cutting the underlying parenchyma, we were able to obtain a 150-200 μm thick lateral wall (LW) tissue of lateral ventricle (LV) in the cerebrum. The isolated LWs were dissociated by pipetting them with a trypsin-EDTA solution at 37°C for 30 s. The cells were centrifuged at 2,000 rpm, 7 min, and at room temperature (RT) and were seeded on 24-well plates coated with poly-D-lysine (0.1 mg/ml, P7280; Sigma, USA). The ependymal cell progenitors were cultured in high glucose DMEM (11965092; Gibco), supplemented with 10% fetal bovine serum (FBS), BM-Cyclin (10799050001; Roche, Switzerland), fungizone (amphotericin B, 15290026; Gibco) and gentamicin (G1397; Sigma). The cultures were allowed to expand and they reached confluency within 7 days.

Transfection of membrane-bound GFP (mGFP) or GFP-Deup1 was performed using the Neon Transfection System, an electroporation device (Invitrogen, USA). The electroporated cells were seeded on glass-bottom dishes (100350; SPL Life Sciences, Korea), coated with poly-D-lysine and laminin (0.02 mg/ml, L2020; Sigma) and cultured in high glucose DMEM containing 10% FBS without antibiotics for 1-2 days. Upon becoming 100% confluent, their medium was changed to high glucose DMEM with 0% FBS to induce differentiation of the ependymal cells.

For immunostaining of the *in vitro* ependymal cells, the cells on the confocal dish were fixed with 4% paraformaldehyde (PFA) and 2% sucrose in phosphate-buffered saline (PBS) for 15 min on ice. The cells were then washed three times with PBS for 5 min each and blocked with 3% bovine serum albumin (BSA), 5% horse serum, and 0.1% Triton X-100 in PBS for 30 min at RT. Next, the cells were stained with various primary antibodies diluted in 3% BSA in PBS overnight at 4°C. The following primary antibodies were used: mouse IgG2a anti-Centrin (1:500, 04-1624; Millipore, USA), mouse IgG2b anti-SAS6 (1:500, sc-81431; Santa Cruz Biotechnology, USA), rabbit anti-CP110 (1:500, A301-343A; Bethyl Laboratories, USA), rabbit IgG anti-CEP164 (1:500, HPA037606; Atlas Antibodies, Sweden), mouse IgG1 anti-GT335 (1:500, AG-20B-0020; AdipoGen Life Sciences, USA), and mouse IgG1 anti-ZO-1-647 (1:1,000, MA3-39100-A647; Invitrogen). Following the primary antibody incubation, the cells were washed and treated with species-specific Alexa Flour 488, 568 conjugated secondary antibodies for 2 h at RT. After washing with PBS, the cells were then coverslipped using VECTASHIELD HardSet (H-1400; Vector Laboratories, USA), an anti-fade mounting medium.

Time lapse imaging analysis

Post 2 days of serum starvation, GFP-Deup1 transfected cells in a glass-bottom dish (SPL Life Sciences) were analyzed. The dishes were placed in an incubation chamber for control of temperature and ambient gas (37°C using the CU-501 controller and 5% CO_2 through the FC-5N gas mixer, provide by LCI Bio, Korea). The cultured cells were imaged using a confocal microscope (LSM700; Zeiss, Germany) equipped with a Plan-Apochromat 63×/1.46 Oil immersion objective lens, an Axio Observer camera (Zeiss) and the appropriate filter set for 488 nm laser wavelength recording. GFP-positive puncta at the early phase of centriole amplification were recorded at 15-min time intervals and were autofocused by applying the definite focus mode. The exported movies were edited using the DaVinci Resolve 17, a video editing application (Blackmagic Design, USA).

In utero electroporation

In utero electroporation of LWs was performed as described (Ryu et al., 2021). Briefly, an E15.5 timed pregnant ICR female (Hsd:ICR(CD-1)) was anesthetized with 2% isoflurane (Hana Pharm Co., Korea) and the uterine horns were exposed by abdominal incision. GFP-Deup1 (2.0 μg/μl) in 0.1% Fast Green dye solution was injected (1-1.2 μl) into the left LV of the E15.5 embryo via a microcapillary. TdTomato expres-

sion vectors (2.0 μg/μl) were injected into the right LV as a reporter. For electroporation, the positively charged (anode) electrode was placed on the left hemisphere and the negatively charged (cathode) on the right hemisphere. Then, 40 voltage pulses were applied 5 times separated by 950 ms for each embryo using a BTX ECM830 electroporator (Harvard Apparatus, USA). After the electroporation, the uterine horns were reinserted into the abdomen cavity and the peritoneum and skin were stitched compactly using a chromic suture (17 mm; Ailee Co., Korea) and a braided silk suture (1.5 Ph, Mersilk W501H; Ethicon, USA), respectively. TdTomato-positive pups were selected at P2 or P3, and post sacrifice, their dissected left LWs were examined for the effect of ectopic Deup1 expression.

Whole mount staining of lateral wall

LWs were isolated from mouse brain as previously described (Labedan et al., 2016). The method involved 200-300 μm thick LWs being immersed-fixed in 4% PFA with 0.1% Triton-X-100 at RT for 10 min and washed 3 times for 10 min each in 0.1% Triton-X-100 in PBS. The whole mounts were then incubated for 1 h at RT in blocking solution containing 3% BSA in PBS. Primary antibodies diluted in the same blocking solution were added to LWs at 4°C for over 24 h. The following antibodies were used: rabbit IgG anti-Deup1 (1:250, PAB20522; Abnova, Taiwan), mouse IgG2a anti-Centrin (1:250, 04-1624; Millipore), mouse IgG2b anti-SAS6 (1:250, sc-81431; Santa Cruz Biotechnology), mouse IgG1 anti-β-catenin (1:250, 610153; BD Laboratories, USA), rabbit IgG anti-CEP164 (1:250, HPA037606; Atlas Antibodies), mouse IgG1 anti-GT335 (1:250, AG-20B-0020; AdipoGen Life Sciences), mouse IgG1 anti-ZO-1-488 (1:250, 339188; Invitrogen) and mouse IgG1 anti-ZO-1-647 (1:250, MA3-39100-A647; Invitrogen). After the 24 h incubation, the primary antibodies were washed off 3 times for 10 min each in PBS with 0.1% Triton-X-100. Then, Alexa Flour 488, 568 conjugated secondary antibodies (1:800; Invitrogen) diluted in blocking solution were added to the whole mounts for 2 h at RT. The secondary antibodies were washed off the samples, and the whole mounts were positioned on the center of a microscope slide and mounted with ProLong Gold Antifade Mountant (P36934; Invitrogen) and cover glasses (24 × 60 mm; Deckglaser; ASONE, Japan).

Beads flow assay

An ependymal flow analysis using fluorescent microbeads was conducted as previously described (Mirzadeh et al., 2010). Briefly, the mice having LWs electroporated with mGFP or GFP-Deup1 vectors were sacrificed and their LWs were freshly exposed and their hippocampus, cortex, thalamus, and choroid plexus were removed in 37°C L-15 Leibovits media. The LWs were immobilized on a dissecting dish using 2 pins in fresh L-15 medium. A grinded glass microcapillary filled with FluoSpheres microbeads (2.0 μm diameter, F8827; Invitrogen) in 5% glycerol solution was positioned just above the dorsal-medial surface behind the adhesion area of the LWs. Micro bead solution was carefully ejected using the Cell Tram Oil micro-manipulator (Eppendorf, Germany) and the movements of microbeads were recorded at 200 ms time intervals using the Axio Zoom V16 fluorescent dissection microscope (Zeiss). High-speed video capture of posterior-medial microbead flow was exported through the ZEN blue imaging software (Zeiss) at 5.0 frames per second (fps). The speed of the beads was measured using the manual tracking method in the ImageJ program (ver. fiji-win64).

Fluorescent microscopy acquisition

For immunostaining analysis of the electroporated LWs, confocal microscopy (LSM700; Zeiss) with a Plan-Apochromat 63×/1.46 Oil immersion objective lens (Zeiss) and an Axio Observer camera (Zeiss) was used. Fluorophores were excited at 488, 568, and 647 wavelengths. Images were taken at 0.5 μm Z-stack intervals for 4-6 μm thick volume and 2 × 2 tile scans were set up for acquiring image size of 203.23 μm × 203.23 μm. The Z-stack images were merged with a maximum intensity projection for a 2D representation. All images were processed and analyzed by ZEN blue software (Zeiss).

In vitro transcription of RNA by injecting into Xenopus embryos

For the expression of mouse Deup1 in Xenopus embryos, GFP-Deup1 was cloned into the PCS2+ vector. The plasmids were linearized and mRNA was made for both of these constructs using the mMESSAGE mMACHINE SP6 transcription kit (AM1340; Thermo Fisher Scientific, USA). The product was purified using an RNA isolation kit (Qiagen, Germany). RNA at 100 pg was injected into one-cell embryos (Umair et al., 2021), and morphologically normal embryos were selected for analyzing the differentiation of MCCs in the epidermis.

Statistics

All quantitative data shown in the scattered plots are presented as mean ± SD values. A two-tailed unpaired *t*-test was conducted using Prism 8.4.3 software (GraphPad Software, USA). Statistical significance is expressed as asterisks on the plots: $*P < 0.05$, $**P < 0.01$, $***P < 0.001$, and $****P < 0.0001$.

RESULTS

Cells expressing Deup1 can be divided into two types

A recent study suggests that Deup1 may not be critical for centriole amplification in ependymal cells or other MCCs (Mercey et al., 2019b). In order to investigate the role of Deup1 in the differentiation of ependymal cells, we transfected GFP-Deup1 into proliferating ependymal precursors and induced differentiation by serum starvation (Nanjundappa et al., 2019; Weibel et al., 1986) (Fig. 1A). At differentiation day (dd) 3, we observed cells with one or two GFP-positive puncta, which were approximately 300 nm in diameter, similar to deuterosomes (Dirksen, 1971; Winey and O'Toole, 2014; Zhao et al., 2013). Importantly, a time-lapse imaging analysis revealed that GFP-positive puncta displayed different behaviors depending on the type of cell. For the type I cell, the puncta remained for several hours before disappearing completely, whereas in the type II cell, puncta became more numerous and then merged together to form large clusters. (Fig. 1B, Supplementary Movie 1). At dd5, we observed that

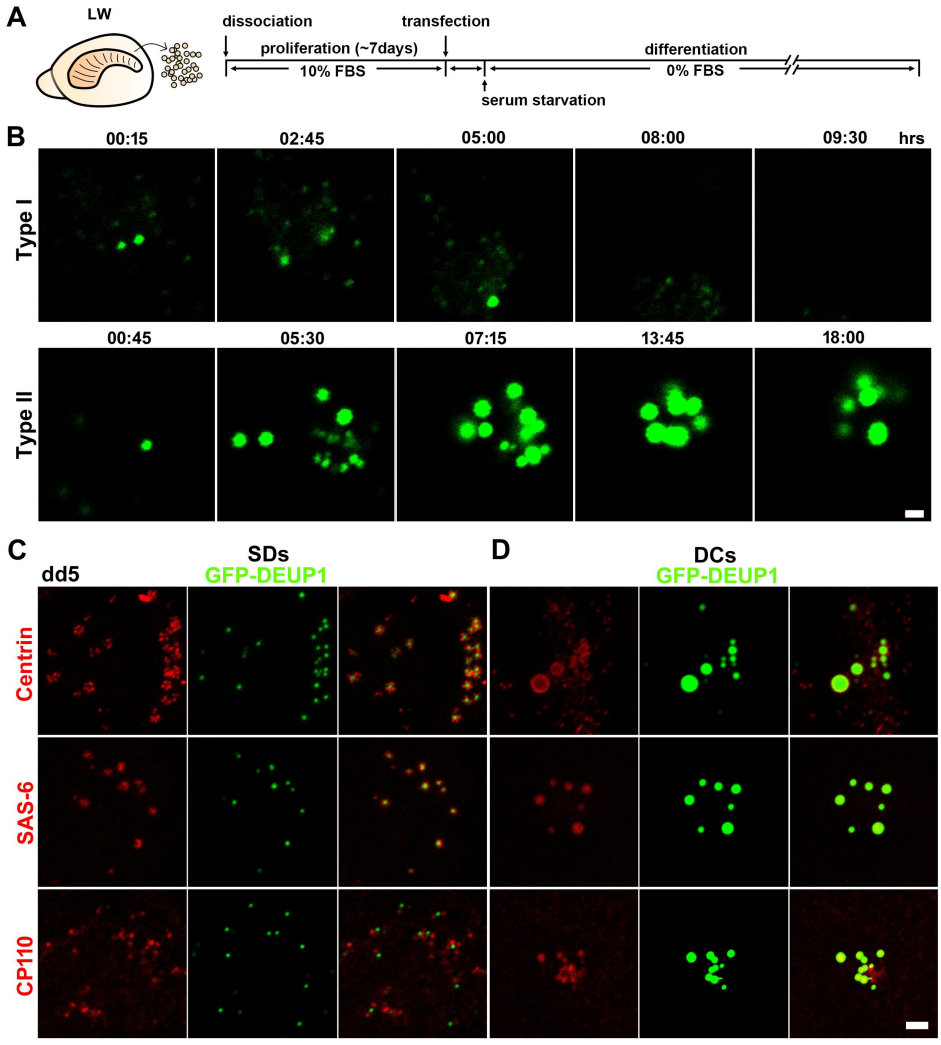

Fig. 1. Two different patterns of Deup1 protein form and aggregate in primary ependymal cells. (A) Schematic diagram illustrating the culture of primary ependymal cells using mouse brain LW at P1 or P2. LW, lateral wall; FBS, fetal bovine serum. (B) Live imaging analysis of cells expressing Deup1. The time-lapse confocal microscope was used to capture images every 15 min of cells with GFP-positive deuterosome-like structures. Scale bar = 1 μm. (C and D) Analysis of the colocalization of GFP-Deup1 puncta with other centriole markers, Centrin, SAS-6, and CP110. The Deup1 puncta are distributed as deuterosome-like structures (SDs) or clustered as much larger aggregates (DCs). The images were taken using a confocal microscope at differentiation day 5 (dd5). Scale bar = 2 μm. SDs, scattered deuterosomes; DCs, deuterosome clusters.

each Deup1 aggregate in type I cells was surrounded by Centrin, SAS-6, and CP110, well-known markers of centrioles (Breslow and Holland, 2019; Kim et al., 2018). These suggested that the Deup1 aggregates represent scattered deuterosomes (SDs), as previously described (Zhao et al., 2013; 2019) (Fig. 1C). Contrary to this, the type II cells containing large Deup1 complexes (0.5-2 μm in their diameter) appear to contain centriole markers within their spherical structures (Fig. 1D). In the type II cells, based on the unique behavior of GFP puncta, we refer to the large Deup1-positive structure as a deuterosome cluster (DC). We observed that, at dd5, the type I cells constituted 39.62% (21/53), whereas the type II cells constituted 60.38% (32/53) in the counted fields. We also examined the mGFP transfected cells. The GFP signals, however, were generally smeared in these cells, and the irregularly GFP-positive puncta barely colocalized with DEUP1 or other markers of centrioles (Supplementary Fig. S1), indicating that the cells transfected with mGFP do not contain GFP-positive DCs and deuterosomes.

To further investigate whether these two distinct cell types undergo the same differentiation process, we allowed the ependymal differentiation to continue until dd14 before conducting immunostaining analyses using antibodies for CEP164, GT335, and ZO-1, which identify BBs, cilia, and apical surface boundaries, respectively (Gonzalez-Mariscal et al., 2000; Mirvis et al., 2018; Wloga et al., 2017) (Figs. 2A-2D). For control, mGFP was transfected into cells, and approximately 90% of the cells were easily classified as either being MCCs or primary ciliated cells (PCCs). In each microscopic field, the proportion of each cell type regardless of the level of GFP signal was measured. Approximately 46.4% of the cells in this control experiment were MCCs, while 39.4% of the cells were PCCs (Figs. 2E and 2F). In contrast, for GFP-Deup1 transfected cells, 36.4% were MCCs and 49.5% were PCCs in the measured fields. These results indicate that the expression of Deup1 prevents the differentiation of ependymal precursors into MCCs. Furthermore, as 65% of the cells with DCs (114/175) were PCCs, it suggested that the DC formation has a negative effect on differentiation of MCCs.

In the ependymal tissue, a small number of cells expressing Deup1 harbor DCs

There was the possibility that DCs resulted from transfection of GFP-Deup1 into ependymal precursors in our culture sys-

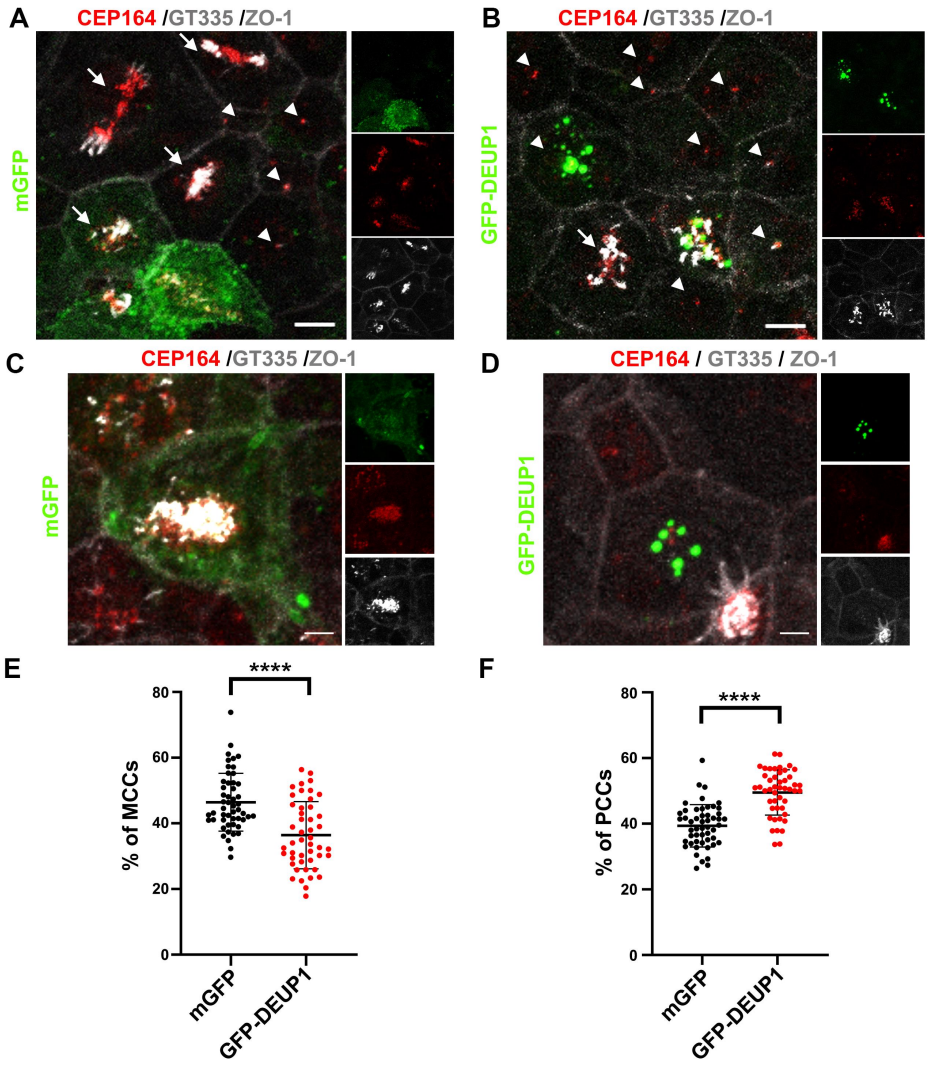

Fig. 2. Gain-of-function of Deup1 inhibits the differentiation of ependymal precursor cells into multiciliated cells *in vitro*. (A and B) Confocal microscopy analysis of ependymal cells at differentiation day (dd) 14. Transfected cells with mGFP or GFP-Deup1 were analyzed with GFP signals in green, BBs with CEP164 in red, cilia with GT335 in gray, and cell boundaries with ZO-1 in gray. The right panel shows each fluorescence at a low magnification. Scale bars = 10 μm. (C and D) Representative images of transfected cells showing BBs (red, CEP164) and cilia (gray, GT335). It is noteworthy that most of the Deup1 transfected cells had GFP-positive DCs at this stage of differentiation. Scale bars = 5 μm. (E and F) MCCs and PCCs were quantified in each field regardless of GFP signal. The data are presented as mean ± SD. For the mGFP control arm, n = 51 fields were collected from 12 plates; for the GFP-Deup1 group, n = 47 fields were collected from 11 plates. The data were compared using a two-tailed *t*-test. ****$P < 0.0001$. BBs, basal bodies; DCs, deuterosome clusters; MCCs, multiciliated cells; PCCs, primary ciliated cells.

tem and that they did not reflect an authentic structure in the brain. In order to rule this out, we examined the Deup1-positive structures in various postnatal stages of the mouse brain LW of LV (Mirzadeh et al., 2010). Our whole-mount immunohistochemical staining analysis demonstrated that SDs were the most frequent type among Deup1-positive cells with 300 nm in diameter, as previously described (Anderson and Brenner, 1971; Winey and O'Toole, 2014; Zhao et al., 2013). They were surrounded by SAS-6 and Centrin (Figs. 3A and 3E), and cells that were SD-positive were more prevalent around P5 (Fig. 3B). However, the prevalence of these cells gradually decreased as postnatal development progressed. It is also important to note that a small number of Deup1-positive cells contained DCs, which were 700 nm to 2 μm in diameter and co-localized with SAS-6 and Centrin (Figs. 3C and 3F). In the postnatal period, DC-positive cells were approximately seven times less abundant than SD-positive cells, and their peak occurred earlier than SD-positive cells (Figs. 3B and 3D). In summary, these results indicate that endogenous expression of Deup1 is transient in differentiating ependymal cells and that DCs are restricted to a small number of these cells.

Ectopic expression of Deup1 in the ependymal tissue inhibits the differentiation of MCCs

In order to examine whether the ectopic expression of GFP-Deup1 enhances the number of DC-positive cells in the differentiating ependymal tissue, we conducted *in utero* electroporation experiments. At embryonic day 15.5, we injected mGFP or GFP-Deup1 constructs into the LV and were electroporated into their LWs (Fig. 4A). We first examined whether DC-positive cells can be observed in the LWs of the injected pups at P5 (Fig. 4B). As expected, approximately 56.57% of GFP-positive cells contained DCs in the Deup1 electroporation group, but none of the GFP-positive cells contained DCs in the mGFP transfection group (Fig. 4C). We allowed the pups to mature until P30 and then assayed the LWs for ependymal differentiation for CEP164 and β-catenin levels, which mark BBs and adhesion junctions, respectively (Bienz, 2005) (Figs. 4D and 4G). The GFP-positive cells in the control electroporation group were consistently detectable and most of these cells were MCCs. In contrast, for the GFP-Deup1 electroporation group, the GFP-positive cells were scarce; this could be due to GFP-Deup1 being susceptible to degradation

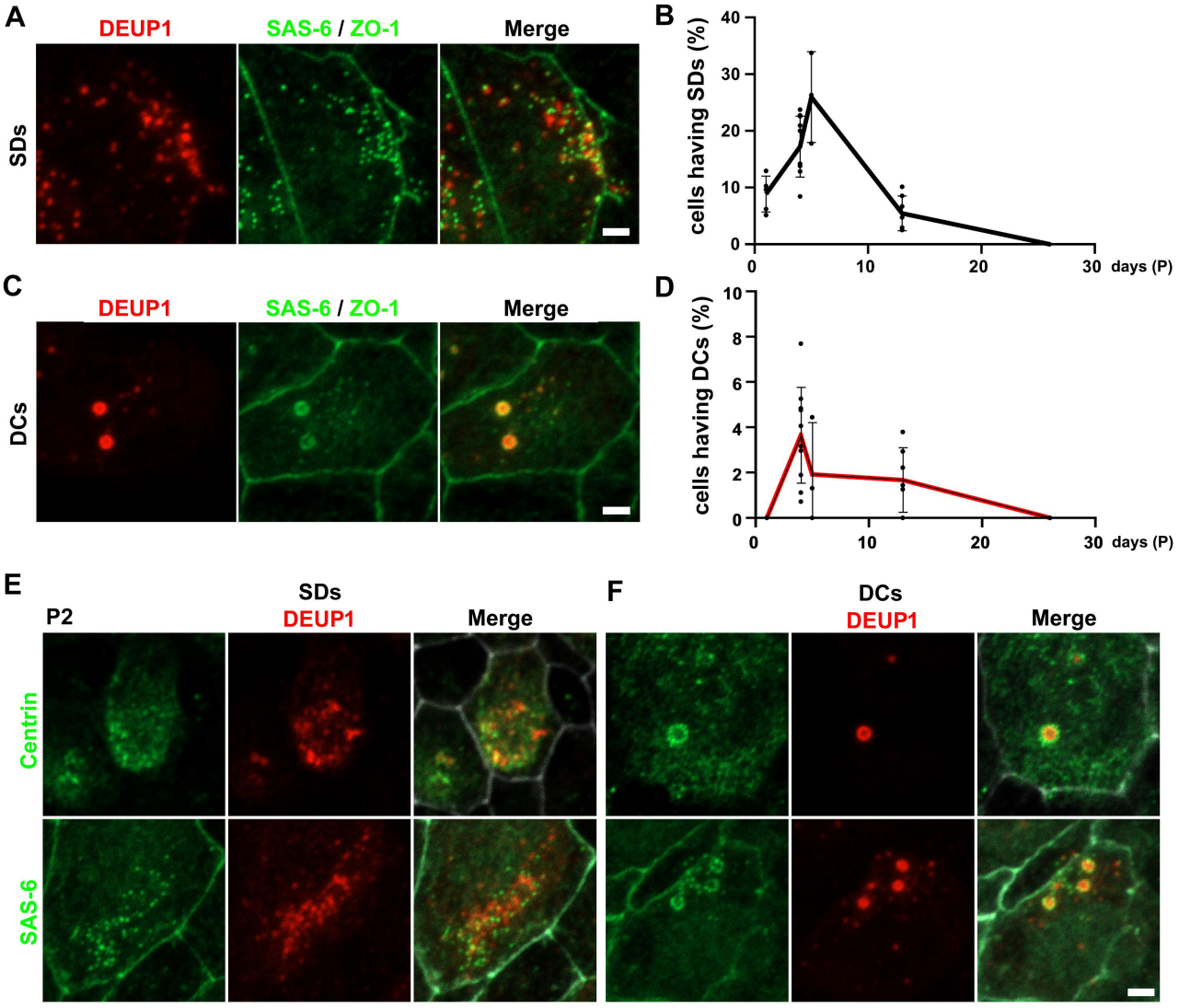

Fig. 3. Deuterosomes are transiently present in differentiated ependymal cells *in vivo*. (A and C) Whole mount staining of LWs using Deup1, SAS6, and ZO-1 antibodies at P2. Scale bars = 2 μm. (B and D) LW associated SDs and DCs were quantified in each field from mice at P1, P4, P5, P13, and P26. SD-positive cells increased up to 25.95% at P5 and no longer existed for the P26 samples. A very small number of DC-positive cells were observed at P4, reaching 3.65% in the counted. The data are presented as mean ± SD. (E and F) Whole mount staining of LWs for Deup1 and Centrin (top panels) or Deup1 and SAS6 (bottom panels). To mark the boundary of each cell, staining with ZO-1 antibody (green) was performed. Scale bar = 2 μm. LW, lateral wall; SDs, scattered deuterosomes; DCs, deuterosome clusters.

during ependymal cell maturation (Fig. 4D). It is important to note that the BB patch in each cell was abnormally formed in the GFP-Deup1 expression group as the BBs were scattered into small clusters or were only aligned along the perimeter of the circle (Figs. 4E and 4F). The Deup1-electroporated tissues had hardly any GFP signal in them, so we quantitated MCCs and PCCs regardless of the GFP signal in each microscopic field, and the cells with defective BB patches were not included in the MCC measurements (Fig. 4G). As a result, we found that the PCC numbers increased in the Deup1 electroporation group, while MCCs levels decreased (Figs. 4H and 4I). Taken together, our results indicate that ectopic expression of Deup1 interferes with the normal development of multiciliated ependymal cells in the brain.

Deup1 expression in ependymal tissues impairs the normal flow of CSF

As a further test of whether ectopic expression of Deup1 in the LW disrupts the normal flow of CSF as a result of both increased PCCs and defective BB patches, we conducted a bead flow assay. For this experiment, fluorescent microbeads were dropped onto a region where GFP expression was abundant (Fig. 5A). As an example, the beads placed just behind the adhesion area moved in a dorsal to ventral direction, and this pattern has been defined as a posterior-medial (PM) flow as in previous studies (Ryu et al., 2021). Importantly, we

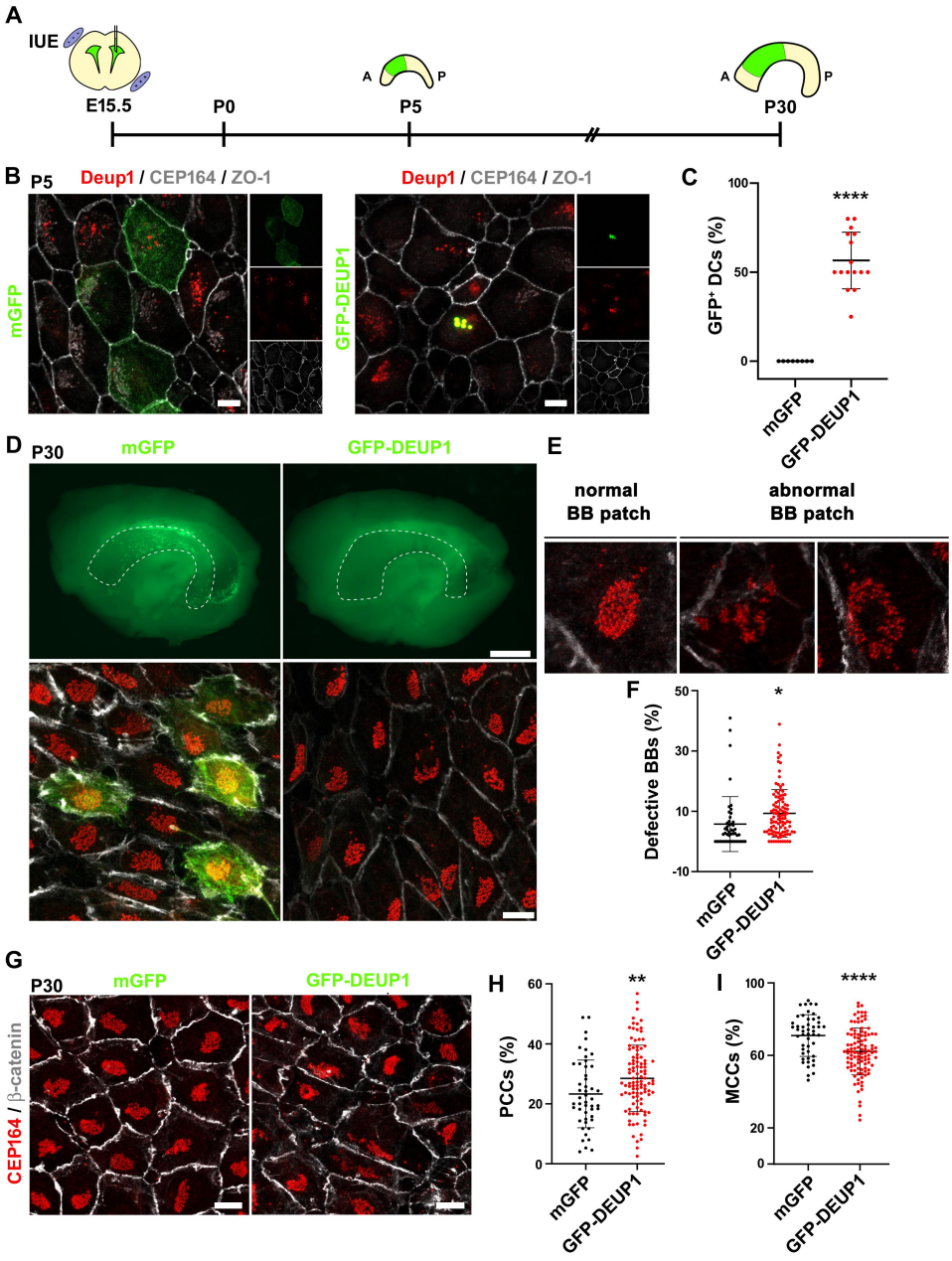

Fig. 4. Deup1 expression in ependymal tissue disrupts ependymal differentiation to multiciliated cells (MCCs). (A) Schematic illustration of an *in utero* electroporation (IUE) experiment. In the lateral wall (LW) region marked with green color, GFP is abundantly observed in the region analyzed. A, anterior; P, posterior. (B) Whole mount staining of electroporated LWs using Deup1, CEP164, and ZO-1 antibodies at P5. mGFP-transfected cells showed a broad pattern of green signal within each cell, while GFP-Deup1 transfected cells showed distinct GFP-positive deuterosome clusters (DCs). Scale bars = 5 μm. (C) The data presented in B were used to calculate the percentage of cells with GFP-positive DCs in each microscopic field. In the mGFP group, 35 GFP-positive cells from two injected mice were analyzed; in the GFP-Deup1 group, 80 GFP-positive cells from three injected mice were analyzed. The data are presented as mean ± SD. $****P < 0.0001$. (D) Fluorescent images of the electroporated LWs at P30 at low magnification. In contrast to the mGFP signals in control cells, GFP signals were barely visible in the LWs electroporated with GFP-Deup1 (top panel). Scale bar = 1 mm. Furthermore, whole mount staining of LWs using CEP164 (red) and β-catenin (gray) antibodies also revealed an identical result (bottom panel). Scale bar = 10 μm. (E) Images of normal or abnormal basal body (BB) patches in LWs electroporated with GFP-Deup1. (F) A quantitative analysis was performed on the percentage of cells with abnormal BB patches. The GFP control group had 5.76% of cells with defective BB patches, while the GFP-DEUP1 group had 9.33% of cells. The data are presented as mean ± SD. $*P < 0.05$. (G) Confocal microscopic image of CEP164 and β-catenin staining. Scale bars = 10 μm. (H and I) The numbers of primary ciliated cells (PCCs) and MCCs were determined based on their CEP164 staining and normalized by the total number of cells in each field. Note that cells with an abnormal BB patch were not included for PCC or MCC counts. The data are presented as mean ± SD. $**P < 0.01$, $****P < 0.0001$. For the mGFP group, n = 48 fields from 5 mice, and for the GFP-DEUP1 group, n = 105 fields from 11 mice were examined.

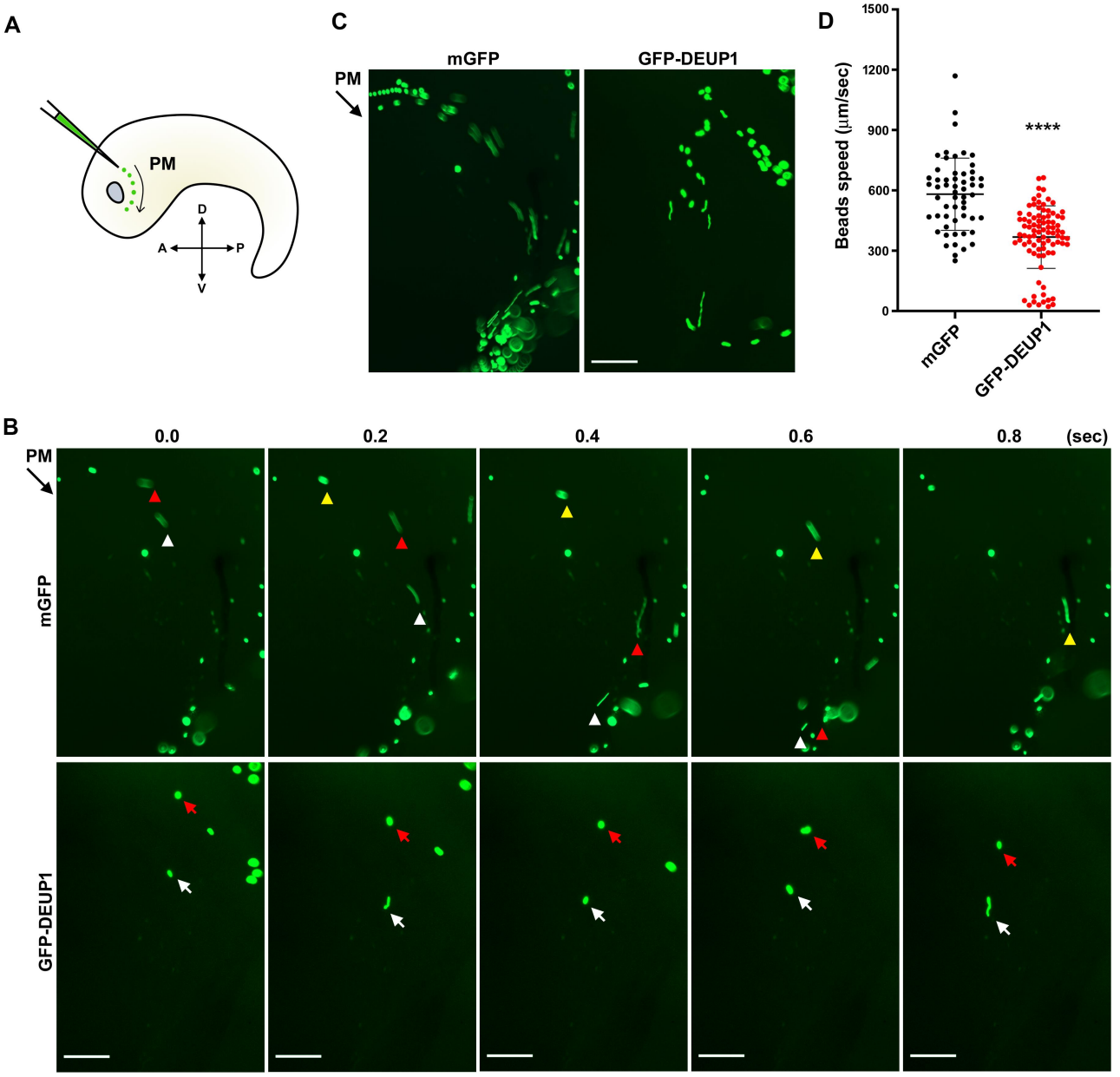

Fig. 5. Ectopic expression of Deup1 impairs the normal flow of cerebrospinal fluid in the ependymal tissue. (A) Diagram depicts the movement of fluorescent beads (green). In this illustration, the flow of beads is in the posterior-medial (PM) direction, right behind the adhesion area (shown in gray). A, anterior; P, posterior; D, dorsal; V, ventral. (B) A high-speed video imaging analysis of each fluorescent bead at different time points. In the mGFP group, each bead is represented by an arrowhead of a different color; similarly, in the GFP-DEUP1 group, each bead is marked with an arrow of a different color. (C) A single image was generated by merging 17 consecutive frames taken at 200 ms intervals. Scale bars = 100 μm (B and C). (D) The speed of each microbead was calculated. The data are presented as mean ± SD. ****$P < 0.0001$. For the mGFP group, n = 56 beads from 6 mice; for the GFP-DEUP1 group, n = 88 beads from 8 mice.

discovered that the flow of beads was stagnant, slow, and floating above in the Deup1 electroporation group (Figs. 5B-5D, Supplementary Movie 2). Overall, our results suggest that Deup1 plays a negative role in ependymal cell differentiation and that the maturation of ependymal cells is dependent on a process that degrades Deup1.

Expression of GFP-Deup1 in *Xenopus laevis* disrupts MCC differentiation in the epidermis

Multicilia in the Xenopus embryonic epidermis, similar to mouse ependymal MCCs, offer an excellent model for studying cilia biogenesis. It is known that precursors of ciliated cells initiate ciliogenesis during stages 22-28 (Faber and Nieuwkoop, 1994), achieving maturity as MCCs with

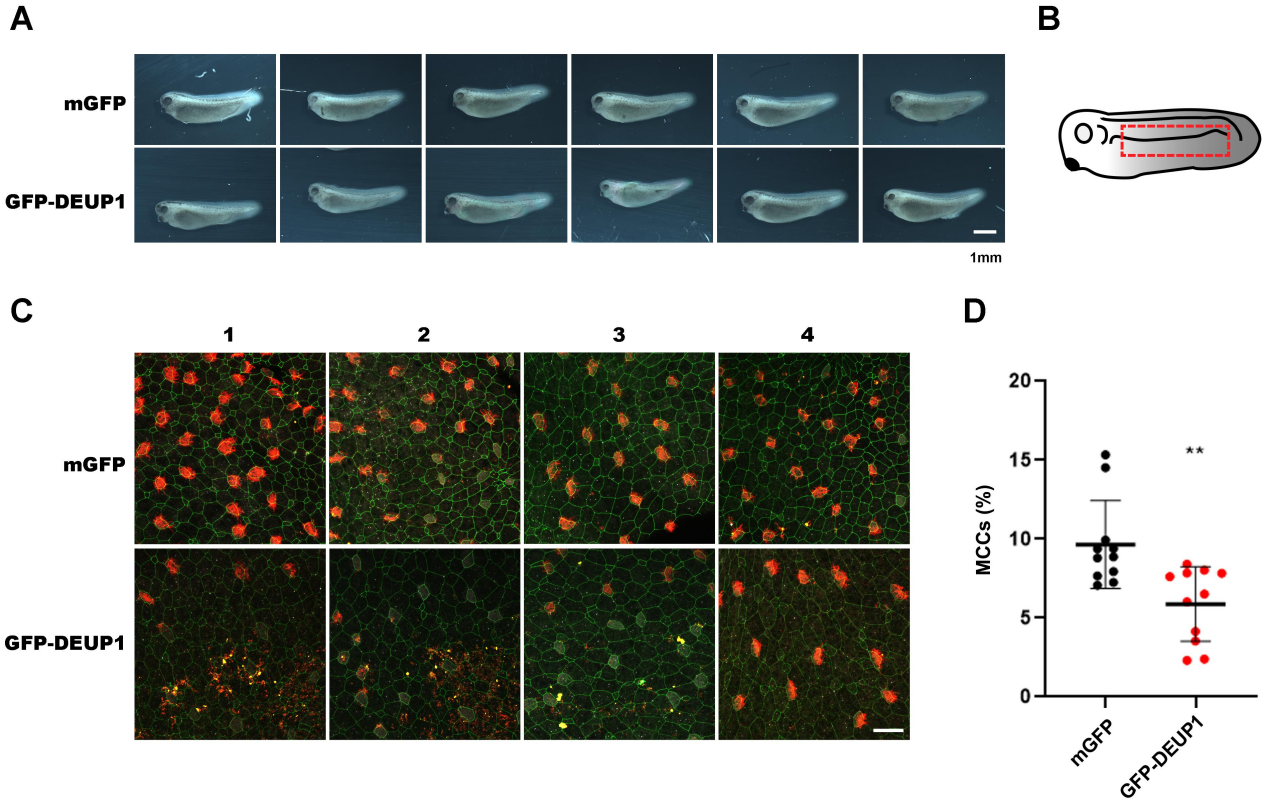

Fig. 6. Ectopic expression of Deup1 in *Xenopus laevis* disrupts the differentiation of multiciliated cells (MCCs) in the epidermis. (A) The diagram shows the overall morphology of various Xenopus embryos at stage 32 after injection of the indicated RNAs. Embryos that were morphologically normal were selected for further immunostaining in this study. Scale bar = 1 mm. (B) This diagram illustrates the region in which differentiated MCCs were analyzed. (C) Whole embryos were immunostained for acetylated tubulin and ZO-1, which serve as markers of multicilia and cell boundaries, respectively. The number on top of each panel represents an independent embryo for each group injected. Scale bar = 50 μm. (D) The number of MCCs in each field was calculated and then expressed as a percentage after dividing by the total number of cells. The data are presented as mean ± SD. $^{**}P < 0.01$. The total number of embryos analyzed for each injection group was 11.

coordinated polarization by stage 30 (Mitchell et al., 2007). In order to determine whether Deup1 expression negatively impacts epidermal MCC differentiation in *X. laevis*, we made *in vitro*-transcribed RNAs for mGFP and GFP-Deup1 (Fig. 6). Injection of 100 pg of either RNA into one-cell embryos did not alter the morphology of Xenopus embryos (Fig. 6A). A number of embryos that were morphologically normal were immunostained with acetylated tubulin antibody and ZO-1, marking their cilia and cell boundary, respectively (Figs. 6B and 6C). On the basis of acetylated tubulin staining, we measured the number of MCCs in each microscopic field. As a result, the MCCs were approximately 10% of mGFP-injected tadpoles, whereas they were 6% in GFP-Deup1-injected tadpoles (Fig. 6D). These results suggest that Deup1 plays an inhibitory role in the differentiation of MCCs across vertebrates.

DISCUSSION

This study shows that deuterosomes with an average diameter of 300 nm undergo two different fates during ependymal differentiation. The first fate is the gradual disappearance of deuterosomes and their absence from mature cells with multicilia. A second fate is for deuterosomes to self-organize into a larger aggregate referred to as a DC. The centriole markers Centrin, SAS-6, and CP110 co-localize with deuterosomes in a manner similar to surrounding a sphere. Unlike deuterosomes, DCs contain centriole markers primarily within a large structure, possibly as a result of a clustering of deuterosomes. A time-lapse imaging analysis consistently showed that a DC can engulf the neighboring deuterosomes to form a larger structure. It is important to note that DC-positive cells tend to become PCCs rather than MCCs, and it is evident that CSF flow is significantly impaired as the proportion of cells with DCs increases in ependymal tissue. We also show that the expression of Deup1 in the epidermis of *X. laevis* interferes with the differentiation of MCCs. We therefore hypothesize that excessive expression of Deup1 is associated with DCs and that the DC may act as a “negative regulator” of multiple centriole production.

The deuterosome has been considered to be a novel platform for generating multiple pro-centrioles. Its unique property is the ability to self-duplicate, and Deup1 is a critical component. A previous study reported the expression of GFP-Deup1 in primary ependymal cells, with a focus on the

generation of multiple deuterosomes under low magnification (Zhao et al., 2019). In particular, the deuterosome mobility was slowed down by nocodazole, a drug that destabilizes microtubules. As a result of this drug treatment, deuterosomes might behave differently than they would naturally, such as disappearing or clustering, as we observed in our experiments. A recent study using Deup1 knockout mice also found that the absence of deuterosomes in MCCs does not affect the number of BBs during differentiation. This implies that the biological role of deuterosomes in MCCs should be studied.

One lead hypothesis for deuterosomes in MCCs is that the deuterosome might act as a temporary storage for pro-centriolar materials that are released when MCCs are required to assemble multiple centrioles at the same time. Since deuterosomes are not involved in the formation of pro-centrioles in this alternative model, the absence of deuterosomes may not affect the total number of BBs in mature MCCs. However, multiple centrioles cannot be assembled simultaneously, thereby affecting the organization of BBs, such as rotational polarity. Our future research will provide further insight into this possibility. Additionally, our results indicate that a small percentage of cells contain DCs, each being a large, spherical structure resulting from the fusion of several deuterosomes. Moreover, these cells show a strong determination to become PCCs. A previous study also revealed the presence of DC-like spherical structures with a diameter of 2 μm in ependymal cells and the interaction of these structures with FOP, pericentrin, and γ-tubulin (Revinski et al., 2018). In this study, it was shown that CDC20B is associated with deuterosomes and that it is required for the cilia production. As a result of CDC20B knockdown, the DC-like structures were observed to increase, disrupting ciliogenesis. This study is consistent with our hypothesis that DCs are physiologically relevant structures that inhibit multiciliogenesis. Consequently, we postulate that DC is a unique structure that contains the components of centrioles and prevents them from being used in the assembly of multiple centrioles.

The results of our *in utero* electroporation experiments demonstrate that ectopic Deup1 expression in ependymal cells is sufficient to enable them to produce DCs at an early postnatal stage but not at a late stage. It has been shown that CDC20B interacts with PLK1, a kinase known to coordinate centriole disengagement with the protease Separase (Revinski et al., 2018). Importantly, over-expression of Separase rescues centriole disengagement and cilia production in CDC20B-deficient MCCs. In this respect, Separase or other proteases might be involved in regulating multiciliogenesis. As an example, the differentiating ependymal cells contain proteases capable of degrading Deup1, and there may be a tug-of-war between Deup1 proteases and Deup1 in order to determine the cell fate of becoming an MCC or a PCC. It is noteworthy that the ependymal tissue displays a pinwheel organization, in which type B1 cells, being primary ciliated adult neural stem cells, are surrounded by several multiciliated ependymal cells (Redmond et al., 2019). In cells with an ependymal fate determination, Deup1 proteases are up-regulated in order to eliminate Deup1-related structures. This degradation may trigger the assembly of multiple centrioles simultaneously. Supporting this hypothesis deuterosomes are transient structures found in differentiated ependymal cells. In this context of a novel role for deuterosome in MCCs, it will be necessary to identify the proteins that degrade Deup1.

Note: Supplementary information is available on the Molecules and Cells website (www.molcells.org).

ACKNOWLEDGMENTS

This work was supported by grants NRF-2021R1A4A1027355, NRF-2021R1A2C3011919, and NRF-2021R1C1C2009319 from the National Research Foundation of Korea (NRF).

AUTHOR CONTRIBUTIONS

M.S. focused on time lapse studies and *in utero* electroporation. J.L. and H.L. performed immunohistochemistry using confocal microscopy. J.K. and V.K. worked on the Xenopus experiments. S.P. designed all the experiments and drafted the manuscript.

CONFLICT OF INTEREST

The authors have no potential conflicts of interest to disclose.

ORCID

Miram Shin https://orcid.org/0009-0008-8201-6140
Jiyeon Lee https://orcid.org/0009-0006-2500-3621
Haeryung Lee https://orcid.org/0000-0002-1539-9259
Vijay Kumar https://orcid.org/0000-0003-1518-196X
Jaebong Kim https://orcid.org/0000-0003-1609-338X
Soochul Park https://orcid.org/0000-0002-7029-3414

REFERENCES

Al Jord, A., Lemaître, A., Delgehyr, N., Faucourt, M., Spassky, N., and Meunier, A. (2014). Centriole amplification by mother and daughter centrioles differs in multiciliated cells. Nature *516*, 104-107.

Anderson, R.G. and Brenner, R.M. (1971). The formation of basal bodies (centrioles) in the rhesus monkey oviduct. J. Cell Biol. *50*, 10-34.

Banizs, B., Pike, M.M., Millican, C.L., Ferguson, W.B., Komlosi, P., Sheetz, J., Bell, P.D., Schwiebert, E.M., and Yoder, B.K. (2005). Dysfunctional cilia lead to altered ependyma and choroid plexus function, and result in the formation of hydrocephalus. Development *132*, 5329-5339.

Bienz, M. (2005). β-Catenin: a pivot between cell adhesion and Wnt signalling. Curr. Biol. *15*, R64-R67.

Breslow, D.K. and Holland, A.J. (2019). Mechanism and regulation of centriole and cilium biogenesis. Annu. Rev. Biochem. *88*, 691-724.

Delgehyr, N., Meunier, A., Faucourt, M., Bosch Grau, M., Strehl, L., Janke, C., and Spassky, N. (2015). Ependymal cell differentiation, from monociliated to multiciliated cells. Methods Cell Biol. *127*, 19-35.

Dirksen, E.R. (1971). Centriole morphogenesis in developing ciliated epithelium of the mouse oviduct. J. Cell Biol. *51*, 286-302.

Faber, J. and Nieuwkoop, P.D. (1994). Normal Table of Xenopus laevis (Daudin) (New York: Garland Science).

Fliegauf, M., Benzing, T., and Omran, H. (2007). When cilia go bad: cilia defects and ciliopathies. Nat. Rev. Mol. Cell Biol. *8*, 880-893.

Gomperts, B.N., Gong-Cooper, X., and Hackett, B.P. (2004). Foxj1 regulates basal body anchoring to the cytoskeleton of ciliated pulmonary epithelial cells. J. Cell Sci. *117*, 1329-1337.

Gonzalez-Mariscal, L., Namorado, M.C., Martin, D., Luna, J., Alarcon, L.,

Islas, S., Valencia, L., Muriel, P., Ponce, L., and Reyes, J.L. (2000). Tight junction proteins ZO-1, ZO-2, and occludin along isolated renal tubules. Kidney Int. *57*, 2386-2402.

Kim, S., Ma, L., Shokhirev, M.N., Quigley, I., and Kintner, C. (2018). Multicilin and activated E2f4 induce multiciliated cell differentiation in primary fibroblasts. Sci. Rep. *8*, 12369.

KIos Dehring, D., Vladar, E., Werner, M., Mitchell, J., Hwang, P., and Mitchell, B. (2013). Deuterosome-mediated centriole biogenesis. Dev. Cell *27*, 103-112.

Labedan, P., Matthews, C., Kodjabachian, L., Cremer, H., Tissir, F., and Boutin, C. (2016). Dissection and staining of mouse brain ventricular wall for the analysis of ependymal cell cilia organization. Bio Protoc. *6*, e1757.

Matsuda, T. and Cepko, C.L. (2007). Controlled expression of transgenes introduced by in vivo electroporation. Proc. Natl. Acad. Sci. U. S. A. *104*, 1027-1032.

Mercey, O., Al Jord, A., Rostaing, P., Mahuzier, A., Fortoul, A., Boudjema, A., Faucourt, M., Spassky, N., and Meunier, A. (2019a). Dynamics of centriole amplification in centrosome-depleted brain multiciliated progenitors. Sci. Rep. *9*, 13060.

Mercey, O., Levine, M.S., LoMastro, G.M., Rostaing, P., Brotslaw, E., Gomez, V., Kumar, A., Spassky, N., Mitchell, B.J., Meunier, A., et al. (2019b). Massive centriole production can occur in the absence of deuterosomes in multiciliated cells. Nat. Cell Biol. *21*, 1544-1552.

Mirvis, M., Stearns, T., and James Nelson, W. (2018). Cilium structure, assembly, and disassembly regulated by the cytoskeleton. Biochem. J. *475*, 2329-2353.

Mirzadeh, Z., Doetsch, F., Sawamoto, K., Wichterle, H., and Alvarez-Buylla, A. (2010). The subventricular zone en-face: wholemount staining and ependymal flow. J. Vis. Exp. *(39)*, 1938.

Mitchell, B., Jacobs, R., Li, J., Chien, S., and Kintner, C. (2007). A positive feedback mechanism governs the polarity and motion of motile cilia. Nature *447*, 97-101.

Nanjundappa, R., Kong, D., Shim, K., Stearns, T., Brody, S.L., Loncarek, J., and Mahjoub, M.R. (2019). Regulation of cilia abundance in multiciliated cells. Elife *8*, e44039.

Ohata, S., Nakatani, J., Herranz-Pérez, V., Cheng, J., Belinson, H., Inubushi, T., Snider, W., García-Verdugo, J., Wynshaw-Boris, A., and Álvarez-Buylla, A. (2014). Loss of Dishevelleds disrupts planar polarity in ependymal motile cilia and results in hydrocephalus. Neuron *83*, 558-571.

Park, S., Lee, H., Lee, J., Park, E., and Park, S. (2019). Ependymal cells require Anks1a for their proper development. Mol. Cells *42*, 245-251.

Redmond, S.A., Figueres-Oñate, M., Obernier, K., Nascimento, M.A., Parraguez, J.I., López-Mascaraque, L., Fuentealba, L.C., and Alvarez-Buylla, A. (2019). Development of ependymal and postnatal neural stem cells and their origin from a common embryonic progenitor. Cell Rep. *27*, 429-441. e3.

Revinski, D.R., Zaragosi, L., Boutin, C., Ruiz-Garcia, S., Deprez, M., Thomé, V., Rosnet, O., Gay, A., Mercey, O., Paquet, A., et al. (2018). CDC20B is required for deuterosome-mediated centriole production in multiciliated cells. Nat. Commun. *9*, 4668.

Ryu, H., Lee, H., Lee, J., Noh, H., Shin, M., Kumar, V., Hong, S., Kim, J., and Park, S. (2021). The molecular dynamics of subdistal appendages in multi-ciliated cells. Nat. Commun. *12*, 612.

Shahid, U. and Singh, P. (2018). Emerging picture of deuterosome-dependent centriole amplification in MCCs. Cells *7*, 152.

Sir, J.H., Barr, A.R., Nicholas, A.K., Carvalho, O.P., Khurshid, M., Sossick, A., Reichelt, S., D'Santos, C., Woods, C.G., and Gergely, F. (2011). A primary microcephaly protein complex forms a ring around parental centrioles. Nat. Genet. *43*, 1147-1153.

Spassky, N. and Meunier, A. (2017). The development and functions of multiciliated epithelia. Nat. Rev. Mol. Cell Biol. *18*, 423-436.

Spassky, N., Merkle, F.T., Flames, N., Tramontin, A.D., García-Verdugo, J.M., and Alvarez-Buylla, A. (2005). Adult ependymal cells are postmitotic and are derived from radial glial cells during embryogenesis. J. Neurosci. *25*, 10-18.

Umair, Z., Kumar, V., Goutam, R.S., Kumar, S., Lee, U., and Kim, J. (2021). Goosecoid controls neuroectoderm specification via dual circuits of direct repression and indirect stimulation in Xenopus embryos. Mol. Cells *44*, 723-735.

Vladar, E.K. and Stearns, T. (2007). Molecular characterization of centriole assembly in ciliated epithelial cells. J. Cell Biol. *178*, 31-42.

Weibel, M., Pettmann, B., Artault, J., Sensenbrenner, M., and Labourdette, G. (1986). Primary culture of rat ependymal cells in serum-free defined medium. Brain Res. *25*, 199-209.

Winey, M. and O'Toole, E. (2014). Centriole structure. Philos. Trans. R. Soc. Lond. B Biol. Sci. *369*, 20130457.

Wloga, D., Joachimiak, E., Louka, P., and Gaertig, J. (2017). Posttranslational modifications of tubulin and cilia. Cold Spring Harb. Perspect. Biol. *9*, a028159.

Zhao, H., Chen, Q., Fang, C., Huang, Q., Zhou, J., Yan, X., and Zhu, X. (2019). Parental centrioles are dispensable for deuterosome formation and function during basal body amplification. EMBO Rep. *20*, e46735.

Zhao, H., Zhu, L., Zhu, Y., Cao, J., Li, S., Huang, Q., Xu, T., Huang, X., Yan, X., and Zhu, X. (2013). The Cep63 paralogue Deup1 enables massive de novo centriole biogenesis for vertebrate multiciliogenesis. Nat. Cell Biol. *15*, 1434-1444.